
Article:
Luo, X., Wang, M. orcid.org/0000-0001-9752-270X, Lee, J. et al. (1 more author) (2021) Dynamic modelling based on surface renewal theory, model validation and process analysis of rotating packed bed absorber for carbon capture. Applied Energy, 301. 117462. ISSN 0306-2619

https://doi.org/10.1016/j.apenergy.2021.117462

Dynamic modelling based on surface renewal theory, model validation and process analysis of rotating packed bed absorber for carbon capture

Xiaobo Luo[a], Meihong Wang[a,*], Jonathan Lee[b], James Hendry[b]

[a]Department of Chemical and Biological Engineering, University of Sheffield, Sheffield, UK, S1 3JD

[b]School of Engineering, Newcastle University, Newcastle-upon-Tyne, UK, NE1 7RU

[*]Corresponding author: Tel: +44(0)114 – 222–7160. E-mail: Meihong.Wang@sheffield.ac.uk,

Abstract:

Rotating packed beds can reduce the equipment size and costs in solvent-based carbon capture. However, difficulties are encountered when modelling rotating packed beds , due to turbulent fluid flows inside rotating packed beds and the cross-sectional area of mass transfer unit that change with radius. This study aims to develop a validated dynamic model of an rotating packed bed absorber and to carry out process analysis through steady state and dynamic simulations. Innovatively, the dynamic model was developed based on surface renewal theory for mass transfer. The model can calculate distributed mass transfer coefficients and other key variables related with absorption performance. Experiments were carried out and new experimental data for rotating packed bed absorber under realistic operating conditions were obtained for model validation. Process analysis about the effects of key operational variables such as rotating speed, liquid-gas ratio and solvent concentration on absorption performance was performed with benchmark MEA solvent. It was found that the optimal MEA concentration is around 70wt%. Dynamic simulation results reveal that the RPB absorber has fast responses for process changes. This new distributed dynamic model and the insights obtained through process simulation will promote rotating packed bed technology towards its industrial deployment in large scale carbon capture processes.

Keywords: Post-combustion carbon capture, Process intensification, Rotating packed bed, Surface renewal theory, Process modelling and simulation, Process analysis

1 Introduction

1.1 Background

World Energy Outlook 2017 [1] recommends that carbon capture and storage (CCS) should be deployed very rapidly to achieve the target of limiting average global temperature increase to 2°C in 2050. Solvent-based carbon capture is considered the most promising technology to capture CO_2 emitted from industrial processes [2]. However, CCS requires massive capital investment, and incurs a high energy penalty (known as 'parasitic load') during operation [3, 4]. This could create significant increments in the cost of electricity for end-users and impedes its industrial deployment.

One potential solution is to use process intensification (PI) technology to achieve significant reduction of the capital cost. Rotating packed bed (RPB) [5] is typical PI equipment and could be used for the absorber and the stripper in post-combustion carbon capture (PCC) processes [6]. By introducing a high centrifugal force field, RPBs enable significantly intensified mass-transfer and higher flooding limits [6], which leads to dramatic reductions in the equipment size [7]. Other advantages of RPBs include short residence time and compatibility with high viscous solvents. These features make RPB technology a great choice for solvent-based carbon capture.

1.2 Previous studies

The effect of gravity on absorption performance of gas liquid contact mass transfer process was observed by Podbielniak [8]. Van Krevelen and Hoftijzer [9] first proposed a dimensionless correlation for liquid-phase mass transfer coefficients in packed columns, which highlighted the importance of the gravitational acceleration in determining the nature of the liquid flow inside the packing. Early work[10, 11] developed mass transfer correlations based on experimental approaches. These correlations gave an exponent between 1/6 and 1/3 for the gravity term. Vivian, Brian [12] experimentally determined volumetric mass transfer rates (

$k_L\alpha_e$) that varied with the centrifugal force to a power of 0.41-0.48,with larger values at lower liquid flow rates. Ramshaw and Mallinson [5] demonstrated liquid phase volumetric mass transfer coefficients ($k_L\alpha_e$) in RPBs were 27- 44 times greater than in a stationary column. RPBs are also capable of using high-viscosity solvents, giving them another advantage over stationary columns. In the study by Jassim, Rochelle [13], aqueous monoethanolamine (MEA) solutions with different MEA mass concentrations of 30 wt%, 55 wt%, 75 wt% and 100 wt% were used to achieve intensified absorption of CO_2 using RPBs. However, in order to achieve 90% carbon capture level for the pilot scale rig, two key manipulated operating variables were set extremely, including L/G ratios in range of 10-20 kg/kg and CO_2 lean loadings in range of 0.05-0.1 mol CO_2/mol MEA.

To encourage industrial deployment, reliable prediction models for RPBs are required to do process analysis, process scale-up, feasibility studies and engineering design. Attempts to propose specific mass transfer correlations for RPBs started with Tung and Mah [14]. In their study, the liquid-side mass transfer coefficients for RPBs were derived based on penetration mass transfer theory for conventional stationary packed columns, by replacing the gravity with centrifugal acceleration. Instead of direct use of the correlations for stationary packed columns, Munjal, Dudukovć [15] attempted to derive the calculation method for the average interfacial area of the RPB. Oko, Wang [16] revealed that Tung and Mah [14] correlation has best prediction accuracy for liquid-side mass transfer coefficient. Oko, Wang [16] also found that, in terms of prediction of effective interfacial area, Luo's correlation[17] is more accurate than Onda's correction[18] by comparing the calculation results with experimental data from Luo, Chu [17]. However, the system conditions should be examined when using Luo's correlation because key parameters in Luo's correlation were regressed by assuming that Hatta number[19] $\gg 1$ during experimental data processing.

Limited by the research tools, most of previous researches focused on improving predictions of the key parameters related with the mass transfer. More recent efforts have investigated system performance of RPBs by developing the models in Aspen Plus® and gPROMS® [7, 20]. Joel, Wang [7] proposed modifying the Radfrac block in Aspen Plus® for conventional stationary cylinder packed column to simulate RPBs, by setting an equivalent diameter and user-defined mass transfer correlations coded as Fortran subroutines. In one recent study by Borhani, Oko [20], a first principle steady state rate-based RPB model for the absorber was developed based on two-films theory in gPROMS®. Using those models, process simulations have been carried out to investigate the effects of different rotor speeds, L/G ratios and other key variables on the absorption efficiency of RPBs.

1.3 Motivation for this study

Research efforts have been taken on RPBs by the major research groups as summarised in Wang, Joel [6]. There are also some RPBs operating commercially, for example in the sulphide removal process. However, the design of RPBs still relies on the calculations for height of mass transfer unit (HTU) and the numbers of mass transfer units (NTU) based on gas-side overall mass transfer coefficient. Most studies have focused on improvement of mass transfer correlations and there are few publications working on the process simulation of RPB systems. Compared with conventional packed columns, there are several research gaps in modelling of RPBs that impede their commercial deployment as a sustainable technology.

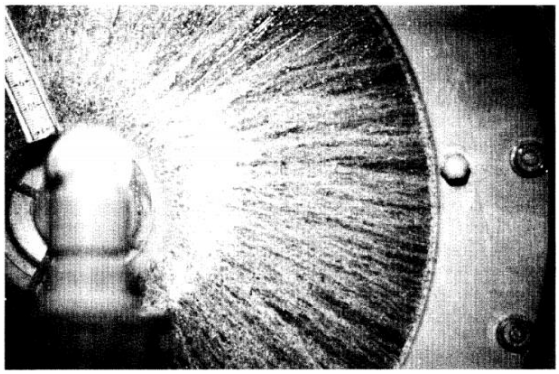

Figure 1. Visual picture of liquid distribution inside an RPB rig[33], Copyright (1996), with permission from Elsevier

The underpinning principle of RPBs is the turbulent flow caused by the centrifugal force, 1-2 orders of magnitude larger than Earth's gravitational force, which intensifies the mass transfer inside RPBs. Burns and Ramshaw [21] conducted a visual study of an RPB and observed droplet flow patterns at designed operational ranges (refer to Fig. 1). However, the methods used to describe mass transfer inside RPBs in previous studies are based on film theories, such as two-films theory and penetration theory, which assume that there exists stagnant "films" between liquid and vapour phases inside the packing. This presupposition has obvious shortcomings and does not reflect the real physical conditions inside RPBs observed empirically. With film theories, interphase mass transfer happens solely by molecular diffusion through "films" regardless of significant convective mass transfer caused by turbulent flows inside PRBs. In this situation, the mass transfer rate calculated based on films theories may be underestimated. Surface renewal theory[22], in contrast, considers mass transfer both by molecular diffusion and convective mass transfer caused by bulk movement and mixing. So, surface renewal theory is physically more accurate than films theories for describing mass transfer inside RPBs.

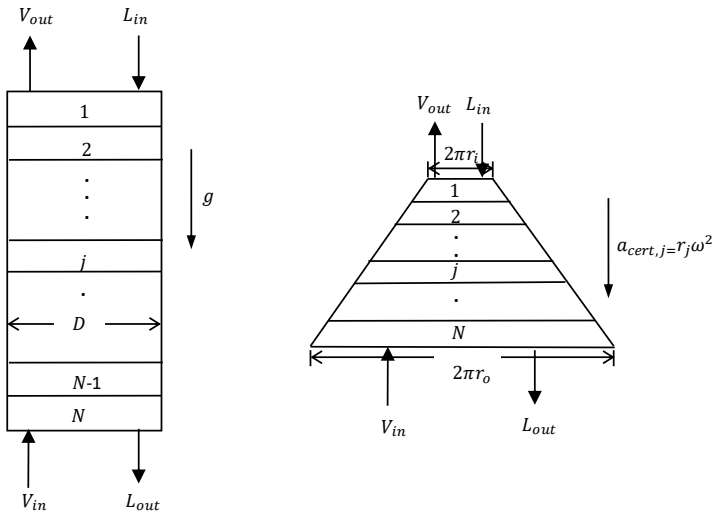

(a) (b)

Figure 2. Sketches of the mass transfer units of (a) a stationary cylinder packed column and (b) an RPB

Another prominent difference between RPBs and stationary columns is that the cross-sectional area of the mass transfer unit inside RPBs changes along radial direction[23]. The ratio of equivalent cross-sectional area at outer side and inner side of RPBs is r_o/r_i (Figure 2) with values in a range of 3 – 5 for current pilot scale plants. This results in significant differences in vapour and liquid loads per volume of mass transfer unit along the radial direction. At the same time, the centrifugal acceleration also varies greatly along the radial direction. The calculations of key mass transfer coefficients and other variables for RPB design are highly non-linear associated with these variables. And more, there are operating envelops for mass transfer inside packed bed. With too low or too high vapour and liquid load, the mass transfer performance decays significantly. In this situation, using mean or average methods to calculate those variables could not reflect the mass transfer phenomenon inside RPBs.

Because of above two gaps at methodology level, previous studies modelling RPBs are on the margin of the goal. Although the experimental approach is still the main scientific way to investigate RPBs, it has several limitations. RPB is a rotating equipment, with rotating speed range of 300 – 1,500 rpm, which results in a high operating cost and potential safety risk (high kinetic energy). At the same time, the scale-up effect is so significant because of aforementioned features of RPBs. For existing RPB test rigs, the size is still too small to draw conclusions about the design of full-scale systems for solvent-based carbon capture based directly on experiments. There are no clear directions for scale-up of this process towards its industrial scale deployment. A reliable model is keenly required, to discover the insights about RPBs, not only for the mass transfer phenomenon but also for the scale-up options and then the process design of industry-scale RPB plants.

1.4 Aim and novel contribution

This study aims to develop a novel dynamic model of an RPB absorber and carry out steady state and dynamic simulations for RPBs in the context of MEA-based carbon capture process. To implement this study, the model is developed for MEA-CO_2-H_2O system using gPROMS ModelBuilder®[24]. The prediction of CO_2 solubility in aqueous MEA solution based on Statistical Associating Fluid Theory-Variable Range (SAFT-VR)[25] equation of state (EOS) was validated with new experimental data.

Four novel features can be claimed for the model developed in this study: (1) the model uses surface renewal theory[22] to describe the mass transfer, consistent with the observed turbulent fluid flows inside RPBs; (2) the model is a distributed model with varied cross-sectional area for RPBs, which enables the predictions of distributed parameters such as mass transfer coefficients, vapour and liquid loads, temperature and pressure profiles inside RPBs; (3) the model is a dynamic process model, which can be used to investigate both steady state (for techno-economical evaluation) and dynamic behaviours (for integration with upstream processes); and (4) new experimental data with realistic operating conditions were used for model validation, which provides more confidence for the model applied in industrial applications. With these novel features, the simulation studies using this model discover some insights for RPBs. They demonstrate a large variation in key parameters along radial direction, fast dynamic response, and an optimum range of MEA concentration in solvent. Those findings could guide the design of large-scale pilot plant and even industrial-scale RPBs to promote this technology, which has great potential for low cost carbon capture.

2 Thermodynamic model prediction and validation

2.1 SAFT-VR EOS

In this study, SAFT-VR[25] EOS is used to model the thermodynamic properties of MEA-H_2O-CO_2 mixture. Mac Dowell, Samsatli [26] well explained the considerations and advantages of using SAFT-VR for modeling of solvent-based carbon capture process. SAFT-

VR provides a molecular-based physical approach to model the chemical equilibrium of the chemistry system, which implicitly express reaction products. In this way, equilibrium reactions are considered in this study. However, even with equilibrium reaction, the model using chemical method, such as e-NRTL, requires to explicitly state all the reactions in the system. Moreover, the enhancement factor [19], E, is required in the film theory based models to reflect the effect of reactions on mass transfer. For both of these tasks, extensive and reliable experimental data is required to describe the reactions. Those data are difficult to obtain, especially for novel solvent and solvent blend. However, using SAFT method only require vapour–liquid equilibrium data to develop the model so that the amount of experimental data required was greatly reduced compared with the chemical approaches [26, 27].

The SAFT-VR parameters of pure components and the binary interaction parameters of MEA-H_2O-CO_2 mixture can referred to the recent study by Brand, Graham [27].

2.2 Validation of CO_2 solubility prediction

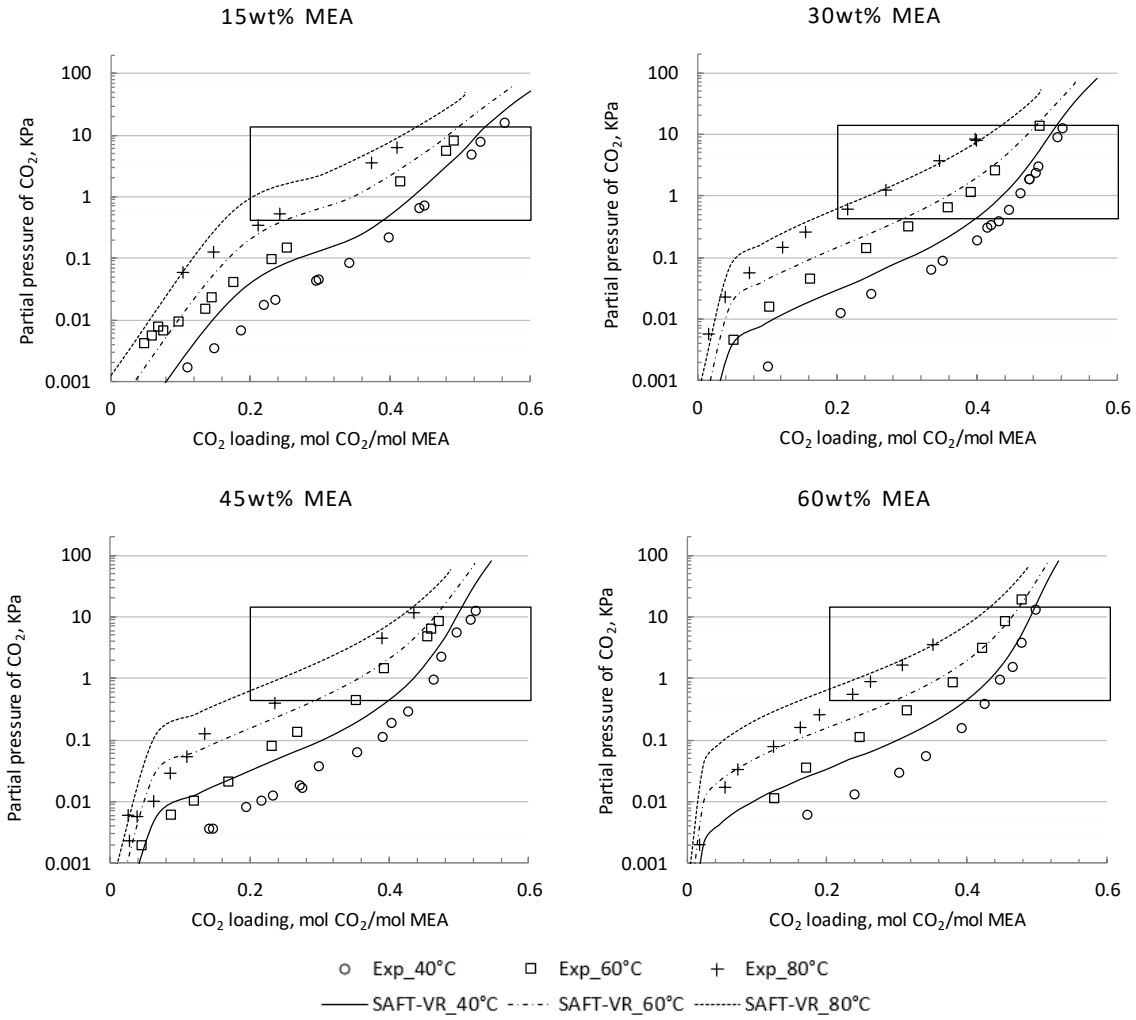

(Note: the rectangle area in each subfigure indicates typical industrial application scenarios with CO_2 partial pressure in the range of 0.45-12 kPa and the CO_2 loading in the solvents of 0.2 - 0.6 mol CO_2/mol MEA.)

Figure 3. CO_2 partial pressure as function of CO_2 loading with 15 wt%, 30 wt%, 45 wt% and 60 wt% MEA solvent

The experimental data of CO_2 partial pressure and/or total pressure of vapour phase at different CO_2 loading in MEA aqueous solution were compared with model predictions. In this study, the experimental data from Aronu, Gondal [28] were chosen for validation purposes. These data cover a wider range of MEA concentrations, temperatures and pressures in comparison to other published sources. The validation results are displayed in Fig. 3. It can be seen that there are some deviations between model predictions and experimental data and they become more

significant in the range of low CO_2 partial pressure. However, the degree of the deviations of VLE predicted by SAFT-VR in this study is similar as those predicted by e-NRTL model by comparing with the validation results from e-NRTL thermodynamic model in the study by Luo and Wang [29].

It is necessary to examine the uncertainties from thermodynamic modelling using SAFT-VR in the context of CO_2 capture processes. The typical CO_2 mole concentration in gas phase is in the range from 0.45% (near the gas outlet of absorber with 90% carbon capture level for the flue gas from natural gas fired power plants) to around 12% (near the gas inlet of flue gas from coal fired power plants), which indicates CO_2 partial pressure in the range of 0.45-12 kPa at atmosphere pressure operating condition for the RPB absorber. At the same time, the CO_2 loading in the solvents is normally in the range of 0.2 - 0.6 mol CO_2/mol MEA (between CO_2 loading in lean solvent and saturated CO_2 concentration in liquid). The absolute percentage errors (APE) of the points within above operating range were calculated and shown in Table 1. It shows that the mean APEs (MAPE) for all cases are less than 5% and the maximum APE is 11.36% for the point at low partial pressure in 60wt% MEA concentration case.

Table 1. Errors of CO_2 solubility prediction in the context of CO_2 capture processes

MEA concentration in lean solvent (wt%)	MAPE	Maximum APE
15	4.54%	6.33%
30	3.66%	9.72%
45	3.53%	6.47%
60	2.80%	11.36%

3 Development of dynamic process model of the RPB absorber

The model development of the RPB absorber in the intensified MEA-based carbon capture process was implemented in gPROMS® ModelBuilder[24]. gPROMS® ModelBuilder offers

substantial flexibility for coding equations to model novel processes, and it has SAFT-VR EOS embedded for the thermodynamic modelling of the MEA-H_2O-CO_2 system.

3.1 Distributed model with varied cross-sectional area

In the newly developed dynamic process model of the RPB, all the variables could be presented in three domains of axial, radial position and time ($x = \mathrm{x}(z, r, t)$). In gPROMS ModelBuilder®, all the variables that are declared within a model are automatically assumed to be functions of time. The other two distribution domains (in this case the axial and radial domains, z and r respectively) have to be specified explicitly for the variables. For the RPB rig modelled in this study, the feeding positions of the flue gas are located in the outside periphery and the feeding positions of the solvent are located in the inside periphery. Inside the packing, liquid and vapour fluids flow counter-currently along radial direction (Seen in Figure 4). In this situation, it is reasonable to assume that the vapour and liquid are evenly distributed at axial directions. Thus, only the radial domain was explicitly specified in the variables.

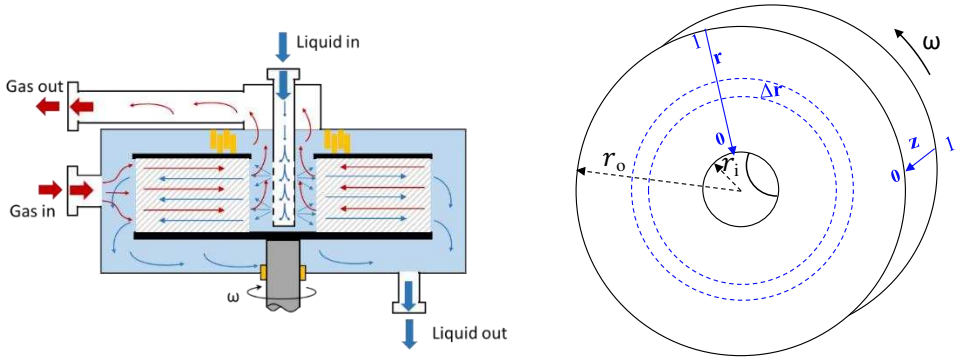

(a) (b)

Figure 4. (a) Sketch of the RPB and (b) Sketch of distributed domain of the packing bed

The following assumptions have been made in modelling this RPB:

- The vapour and liquid distributions are even along axial direction of the packing.
- The liquid bulk and vapour bulk are assumed to be well-mixed.
- Heat loss from the wall of the RPB absorber was neglected due to the small size and modest temperature of the RPB absorber.

- There is no holdup for the vapour phase.
- The gas side mass transfer resistance is neglected.
- Coriolis and gravitational force may be neglected as these forces are of lesser magnitude than the centrifugal force.

3.2 Mass and energy conservations

The governing equations of mass and energy conservations for the RPB absorber were derived from Lawal, Wang [30]. The mass balance for the liquid phase and the vapour phase are presented in Eqs (1) and (2) respectively.

$$\frac{dM_{L,i}}{dt} = \frac{-1}{(r_o - r_i)\cdot A}\frac{\partial F_{L,i}}{\partial r} + N_{IP,i}\cdot MW_i \cdot a_P \cdot \varphi \quad (1)$$

$$0 = \frac{-1}{(r_o - r_i)\cdot A}\frac{\partial F_{V,i}}{\partial r} + N_{IP,i}\cdot MW_i \cdot a_P \cdot \varphi \quad (2)$$

Where, $dM_{L,i}$ is the change of mass holdup in liquid phase of component i, with respect to time; $\frac{\partial F_{L,i}}{\partial r}$ is the differential change of the component mass flow along the radial dimension of the RPB packing; $N_{IP,i}$, is the estimated interphase molar fluxes of each component, which are determined using surface renewal theory as described in Section 3.3; A is the area of mass transfer unit (m^2); a_P is specific surface area of the packing (m^{-1}); MW_i is molecular weight of component i ($g\cdot mol^{-1}$); φ is effective interfacial area ratio.

The energy balance equations for the liquid phase and the vapour phase are presented in Eqs (3) and (4) respectively.

$$\frac{dU}{dt} = \frac{-1}{(r_o - r_i)\cdot A}\frac{\partial F_{L,H}}{\partial r} + a_P \cdot \varphi\left(H_{L,cond} + H_{L,conv} + H_{abs}\right) \quad (3)$$

$$0 = \frac{-1}{(r_o - r_i)\cdot A}\frac{\partial F_{V,H}}{\partial r} + a_P \cdot \varphi\left(H_{V,cond} + H_{V,conv}\right) \quad (4)$$

$$H_{abs} = N_{IP,\ CO_2}\cdot h_{abs} \quad (5)$$

Where, $\frac{dU}{dt}$ is the change in energy holdup with respect to time; $\frac{\partial F_{L,H}}{\partial r}$ is the differential change of 'energy flow' along the radius of the RPB absorber; the liquid heat fluxes at gas-liquid interface including conduction, $H_{L,cond}$, convection, $H_{L,conv}$ as well as the heat flux due to chemical absorption of CO_2, H_{abs}. The specific heat of absorption, h_{abs} (J/mol), is estimated as a function of temperature and CO_2 loading based on expressions in literature[31], presented in Eq. (6).

$$h_{abs} = R\left(-14281 - \left(\frac{1092554\alpha^2}{T}\right) - \left(\frac{6800882\alpha}{T}\right) + 32670.01\alpha\right) \qquad (6)$$

Where, R is the gas constant with a value of 8.314 $(J \cdot K^{-1} \cdot mol^{-1})$; α is the CO_2 loading in liquid phase $(mol\ CO_2 / mol\ MEA)$; T is the temperature of liquid phase (K);

3.3 Interphase mass transfer based on surface renewal theory

Considering the turbulent flow inside RPBs, this study applied surface renewal theory [22] to describe the interphase mass transfer. Surface renewal theory regards the liquid as two regions: a large well-mixed bulk and an interfacial region that is exposed to the gas for different lengths of time and is renewed rapidly (see in Fig. 5).

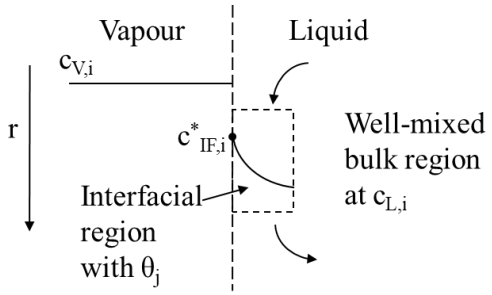

Figure 5. Sketch of interphase mass transfer based on surface renewal theory, adapted from Cussler [32]

At a macro level, the interphase mass transfer rate based on surface renewal has the same formula with the film-based models, which is presented in Eq. (7).

$$N_{IP,i} = k_L a_e (c^*_{IF,i} - c_{L,i}) \qquad (7)$$

Interphase molar flux of component $N_{IP,i}$ is determined based on the liquid mass transfer coefficient $k_L(m \cdot s^{-1})$, effective interfacial area $a_e(m^{-1})$ and the difference between the interfacial liquid-side saturated concentration $c^*_{IF,i}$ $(mol \cdot m^{-3})$ and bulk liquid concentration $c_{L,i}$ $(mol \cdot m^{-3})$ of component i [32]. It should be noted that the interfacial liquid-side saturated concentration $c^*_{IF,i}$ already takes both chemical reactions and physical solubility into account for this reactive absorption process as SAFT-VR EOS was applied. Otherwise, if e-NRTL or another thermodynamic model is chosen, the interfacial liquid-side saturated concentration $c_{IF,i}$ will be calculated only considering the physical phase equilibrium by Henry's Law. In this situation, an enhancement factor [13] needs to be added to include the impact of the reaction to the mass transfer. So the application of SAFT-VR EOS significantly simplifies the calculations, especially for newly developed solvent or blend solvents.

The mass transfer coefficient in Eq. (7) can be calculated by Eq. (8). Detailed derivation can refer to the study by Shen, Xu [33].

$$k_L = (1+s)\left(\sqrt{Ds}\, erf(st)^{0.5} + e^{-st}\sqrt{D/(\pi t)}\right) \tag{8}$$

Where D is the diffusivity of CO_2 in the solvent $(m^2 \cdot s^{-1})$, calculated by using N_2O analogy method given by Versteeg and van Swaaij [34]; s is surface renewal frequency (s^{-1}) and t is gas-liquid contact time (s). erf is the error function.

The surface renewal frequency s was calculated by Eq. (9), cited from the study on rotating discs by Deng and Dai [35]. In their study, the surface renewal in a rotating disk was investigated including main factors for both low and high viscosity systems by using computational fluid dynamics. A correlation equation was presented in expression of the liquid phase Reynold Number and Froude Number, which considers effects of viscosity and velocity in the context of turbulent flows in centrifugal force field. More details can refer to the publication by Deng and Dai [35].

$$s = N\beta\left(\frac{r\omega^2}{g_0}\right)^{-0.1}\left(\frac{\rho_L r^2\omega}{\mu_L}\right)^{0.39} \quad (9)$$

Where N is rotating speed of the RPB motor (s^{-1}); β is a parameter with a value of 0.235 in this study; r is equivalent radius of the mass transfer unit (m); ω is the angular velocity of the mass transfer unit ($rad \cdot s^{-1}$); g_0 is the standard earth gravity acceleration constant with a fix value of 9.807 ($m \cdot s^{-2}$), ρ_L is liquid density ($kg \cdot m^{-3}$); μ_L is liquid dynamic viscosity ($kg \cdot s^{-1} \cdot m^{-1}$).

The gas-liquid contact time, t , can be calculated based on the liquid holdup and the fluid velocities [36] by Eqs. (10) and (11).

$$\varepsilon_L = 0.039\left(\frac{r\omega^2}{g_0}\right)^{-0.5}\left(\frac{V_L}{V_0}\right)^{0.6}\left(\frac{v_L}{v_0}\right)^{0.22} \quad (10)$$

$$t = \frac{\varepsilon_L}{V_L}\Delta r \quad (11)$$

Where ε_L is the liquid holdup ratio, V_L is the superfical liquid velocity ($m \cdot s^{-1}$); V_0 is the characteristic superficial velocity with a fix value of 0.01 ($m \cdot s^{-1}$); ν is kinematic viscosity of liquid ($m^2 \cdot s^{-1}$); ν_o is the characteristic kinematic viscosity with a fixed value of $1 \times 10^{-6}(m^2 \cdot s^{-1})$; Δr is the difference of the radius (m) (refer to Fig. 4(b)).

3.4 The effective interfacial area

For gas liquid interfacial area inside stationary packed column, Onda's correlation [18] is commonly used. Differed from stationary packed column, RPB can be operated at the different rotating speed. The superficial liquid velocity inside RPB changes at the different rotating speed, which should affect the gas-liquid interfacial area inside RPB. At the same time, the specific liquid load varies significantly in the radial direction inside RPB, especially for the small size RPBs which have large values for r_o/r_i. Even when the liquid loads in the inner side of the packed bed are within the operation envelope, the liquid loads in outer side of packing may become too low to wet the packing well.

Considering above reasons, a distribution factor γ was added to the original Onda's correlation[18] for the calculation of effective gas liquid interfacial area (seen in Eq. (12)).

$$\frac{a_e}{a_P} = \gamma\left(1 - \exp\left(-1.45\left(\frac{\sigma_c}{\sigma}\right)^{0.75}\left(\frac{V_L\rho_L}{a_P\mu_L}\right)^{0.1}\left(\frac{{V_L}^2 a_P}{a_c}\right)^{-0.05}\left(\frac{{V_L}^2\rho_L}{\sigma a_P}\right)^{0.2}\right)\right) \quad (12)$$

Where, the distribution factor γ is expressed in Eq. (13).

$$\gamma = a \cdot {a_c}^b\left(1 - \exp\left(-\left(\frac{L_{SLL}}{L_{MWR}}\right)^c\right)\right) \quad (13)$$

The first part of the expression, $a \cdot {a_c}^b$, for the distribution factor (Eq. (12)) accounts for the effect of centrifugal acceleration. The second part of distribution factor, $1 - \exp\left(-\left(\frac{L_{SLL}}{L_{MWR}}\right)^c\right)$, accounts for the effect of liquid load for packing wetting. L_{MWR} $(m \cdot s^{-1})$ is the minimum wetting rate for the liquid load. This depends on packing material and types, according to the expression in Eq.(14), taken from Kister, Haas [37].

$$L_{MWR} = \delta\left(\frac{196.86}{a_P}\right)^{0.5} \quad (14)$$

Where, δ is the minimum wetting rate for different materials of the packing used in RPBs. Its value can be found in Table 1 in Appendix A. L_{SLL} $(m \cdot s^{-1})$ is the specific liquid load, which is the volumetric velocity of liquid per surface area of the packing, calculated by Eq. (15).

$$L_{SLL} = \frac{L}{a_P V_P} \quad (15)$$

Where, L is liquid volume flow rate $(m^3 \cdot s^{-1})$; V_P is the volume of the packing of the separation unit (m^3).

Three parameters, a, b and c, in Eq. (13) were regressed in this study based on 10 experimental cases (Day1_1 to Day1_10 experiment case in Table 2 in Appendix A). The regression was implemented by Least Squares method in Excel with Generalized Reduced Gradient (GRG) nonlinear solver considering that this is a smooth nonlinear problem. After regression, a, b and c get the values of 30.7, -0.631 and 0.2 respectively in this study.

4 Model validation with experimental data

4.1 Experimental rig and analytical method

The process flow diagram of the experimental rig is shown in Figure 6. A synthetic flue gas was produced at 12vol% $CO_{2(g)}$, 12 l/s flowrate, a temperature of 40°C and saturated humidity. Gas premixing is achieved using two gas mass flow controllers, mixing pure CO_2 from a cylinder with a main supply of compressed air. A bubble column humidifier controls temperature and humidity for the synthetic flue gas. The MEA solution was stored in a feed tank, pre-heated to 40°C and preloaded to α = 0.2mol CO_2 /mol MEA. This mimics conditions for lean MEA returning from a typical stripping operation. The MEA is delivered into the centre of the RPB using a gear pump and flowrates are measured using a Coriolis flowmeter. Figure 7 shows the RPB rotor. The RPB rig has a packed bed with an outer diameter of 0.28 m and an internal diameter of 0.08 m. It has a radial packed depth of 0.10 m (i.e. 0.14 m – 0.04 m, equivalent to the height of the packed bed in a conventional absorber column). The packing used in the RPB absorber is Expamet stainless steel mesh, it has a specific surface area of 663 m^2/m^3 and a void fraction of 0.801. The orientation of the rotor axis is horizontal. The RPB absorber can be rotated at speeds of 300 – 1000 rpm. The lean MEA solution enters the RPB via a liquid distributor onto the inner side of the packing. CO_2/air mixture enters the RPB casing from the outer side of the packing.

The performance of the experimental RPB was determined from measurements of CO_2 gas concentrations at the inlet and outlet of the RPB. This used two CO_2 gas analysers Geotech G100, supplied by QED Environmental Systems Ltd., shown as AI in Figure 6. Liquid samples were also tested to close the mass balance. The lean solvent was sampled immediately before the experiment, and the liquid outlet was sampled for each experimental data point. The samples were analysed using a direct titration method based on Chang [38].

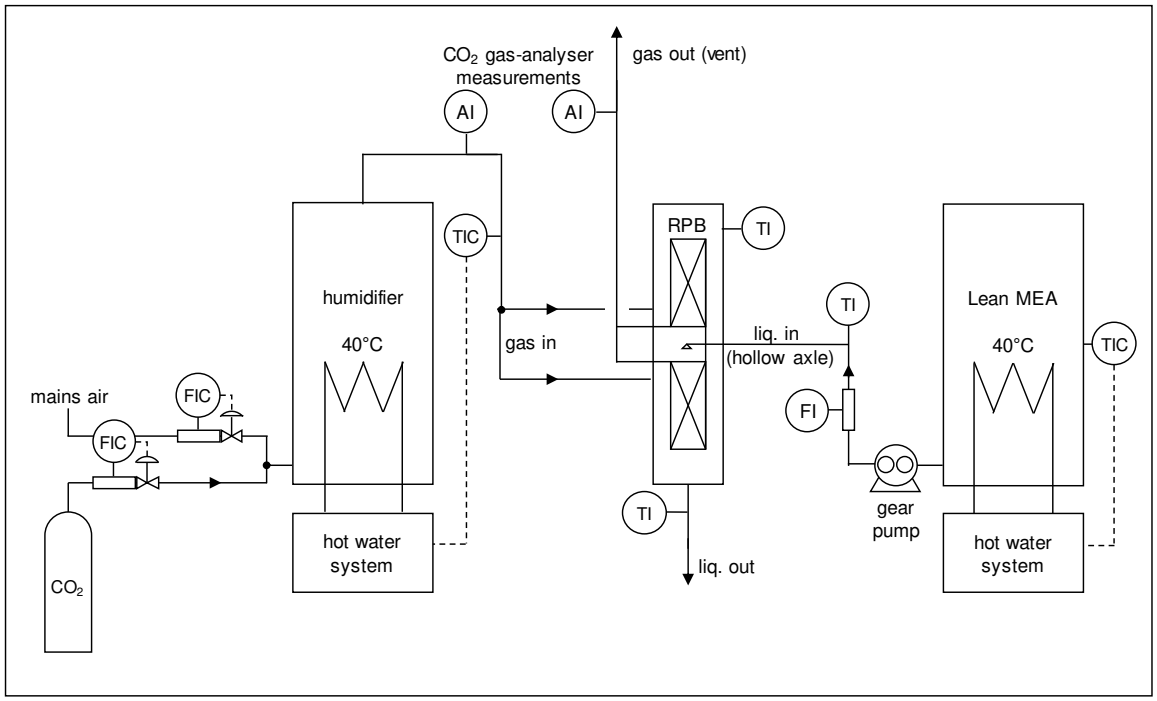

Figure 6. Process flow diagram of the pilot plant

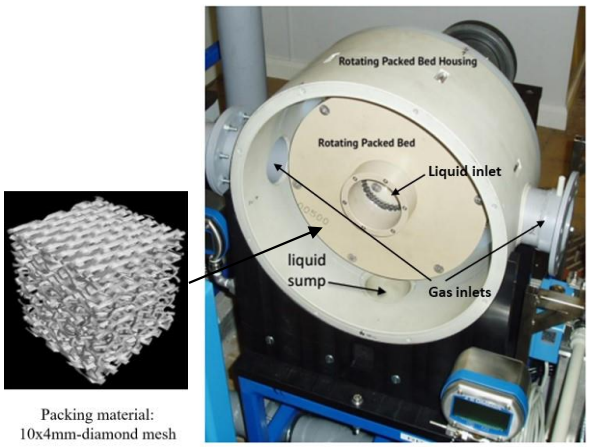

Figure 7. The RPB rig and packing material

The test campaign used 33, 42, 62 wt% MEA solvent to absorb CO_2 from the flue gas with a flow rate of 53 kg/h and CO_2 concentration of 12.0 mol%. The solvent flow rate varied from 105.5 to 317.5 kg/hr and the rotating speeds of the RPB rig were set at 300, 650, 1000 rpm respectively.

4.2 Results from steady state model validation

The experimental data for model validation include the inputs and measurements for all 65 experiment cases (refer to Table 2 in Appendix B). Fig. 8 presented validation results between

experimental data and model predictions on CO_2 mole fraction in gas outlet and on the temperature of liquid outlet. It can be seen that the model predictions are in very good agreement with the experimental data and most of the errors are around 5%. For predictions of CO_2 mole fraction in gas outlet, the largest deviations are from four data points for 62 wt% MEA at 1000 rpm rotating speed and at 5.5 L/G ratio, these have errors around 10.0%. It was also noticed that, in most case, the model predictions of liquid outlet temperature are lower than experimental measurements. One reason may be that the model does not consider the heat generated by pressure loss from the fluids and mechanical friction of the rotation movement.

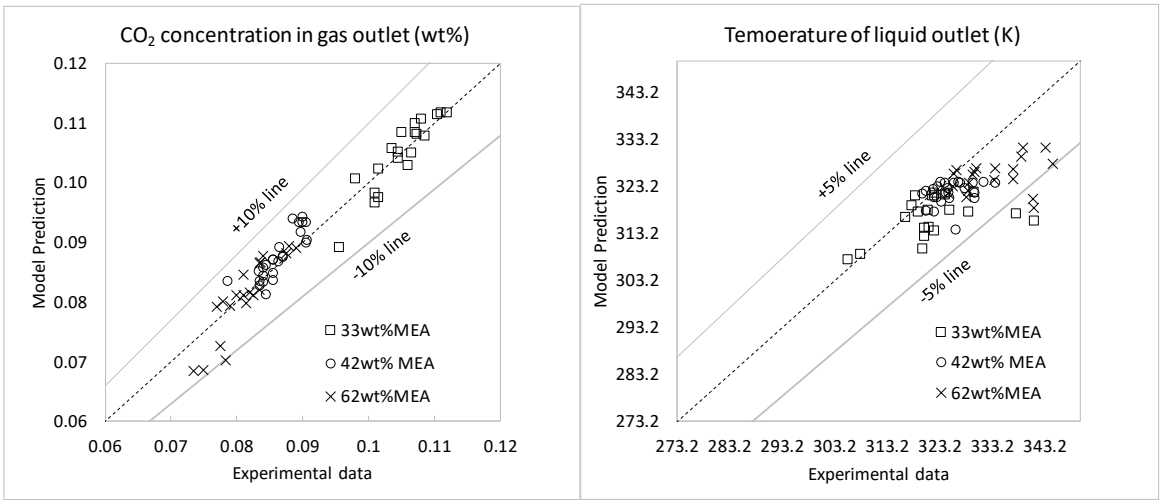

(a) (b)

Figure 8. Validation results by comparing (a) the CO_2 concentration in gas outlet, and (b) the temperature of liquid outlet

5 Process analysis of RPB absorber at pilot plant scale

Using the validated model, steady state and dynamic process simulations were carried out for a RPB at the pilot plant scale with same equipment size as the experiment rig and consistent operating conditions with the test campaign, including (1) CO_2 lean loading in the range of 0.2-0.25 mol CO_2/mol MEA; (2) L/G ratio in the range of 2-6 kg/kg; and (3) rotating speed in the range of 300 – 1450 rpm.

It should be noticed that the CO_2 capture levels were not push to 90% in the case setups in this section considering current research level about RPBs. There are two approaches to push CO_2 capture level to 90%. The first approach is to use extreme operating conditions, such as high L/G ratio and low CO_2 loading. However, that will lead to high energy demands and are not consistent with the industrial applications. The process analysis under these extreme operating conditions may weaken the effects of other variables. The second approach is to increase the height of the packed bed. However, there are few studies on that for RPBs. The scale-up effect could be very significant by simply increasing the height of the packing in RPBs because of the geometric structure of the equipment. It is hard to evaluate the uncertainties at this stage.

5.1 The Base Case

The base case was set up at the pilot plant scale and the inputs and operating conditions are presented in Table 2.

Table 2. Inputs and operating conditions of the base case

Description	Value
Flow rate of flue gas (kg/h)	61.2
Composition of flue gas (mass fraction)	CO_2:0.209; H_2O:0.042; N_2:0.748
Flue gas temperature (°C)	40.0
Flow rate of lean solvent (kg/h)	244.8
MEA concentration in lean solvent (wt%)	50.0
CO_2 loading in lean solvent (mol CO_2/mol MEA)	0.2
Lean solvent temperature (°C)	35.0
Rotating speed (rpm)	650
Operating pressure of the RPB absorber (bar)	1.0

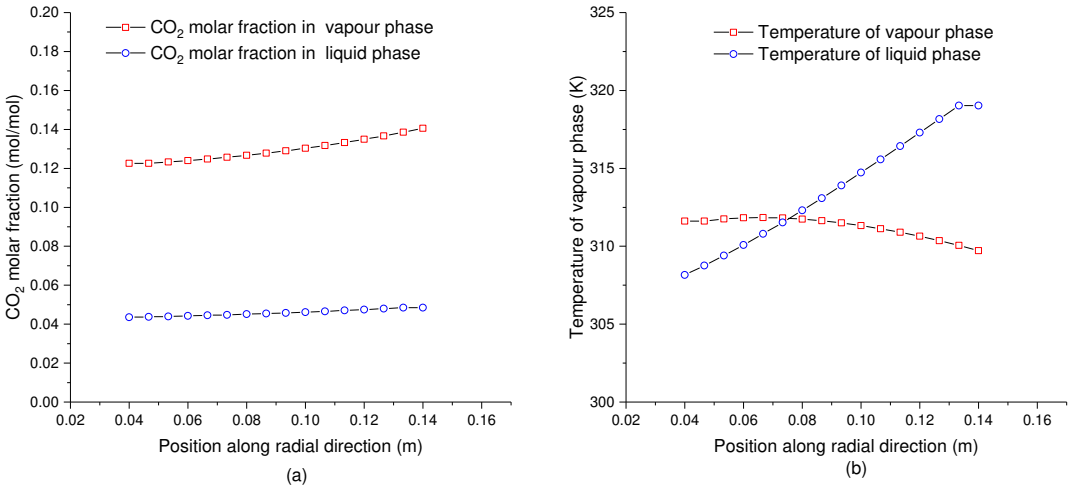

Figure 9. Process simulation results: (a) CO_2 concentration profiles in vapour and liquid phases along radial direction, and (b) temperature profiles for vapour and liquid phases along radial direction.

As the radial depth of the packed bed inside this RPB is only 0.10m (equivalent to the height of packed bed in a stationary column), the CO_2 capture level is around 15.72%. Fig. 9 (a) shows that the changes in CO_2 concentrations are slow in both phases, which means that the driving force for CO_2 mass transfer does not change too much. Fig. 9 (b) illustrates that the liquid temperature sharply from inner side to outer side of the RPB whilst the vapour temperature does not change too much. The vapour temperature at outer side is decided by the gas feeding temperature (40 C° in this case) and the temperature of inner side of RPB is dominated by the liquid feeding temperature (35 C° in this case). In this situation, there usually is an obvious temperature bulge inside stationary CO_2 absorbers. However, the equivalent height of the packed bed is only 10cm in this RPB. The results reflect that heat transfer between vapour and liquid phases are not effective in such short flow path and contact time.

Fig.10 (a) shows change of the centrifugal acceleration in proportion to the radius, which has large impacts on mass transfer relevant parameters. Fig.10(b) indicates that the effective interfacial area ratio varies significantly along radial direction inside the RPB absorber. One reason may be that the liquid load changes as a result of varying cross-sectional area, and it

may be in a good operating point in the inner side of the packing but could decrease to a value lower than the minimum wetted rate near the outer side. Fig.10(c) illustrates the increase in surface renewal frequency from inner side to outer side of the packing. The centrifugal acceleration promotes fluid turbulence, which accelerates the surface renewal. Fig.10(d) depicts the liquid mass transfer coefficients along radial direction inside the RPB absorber.

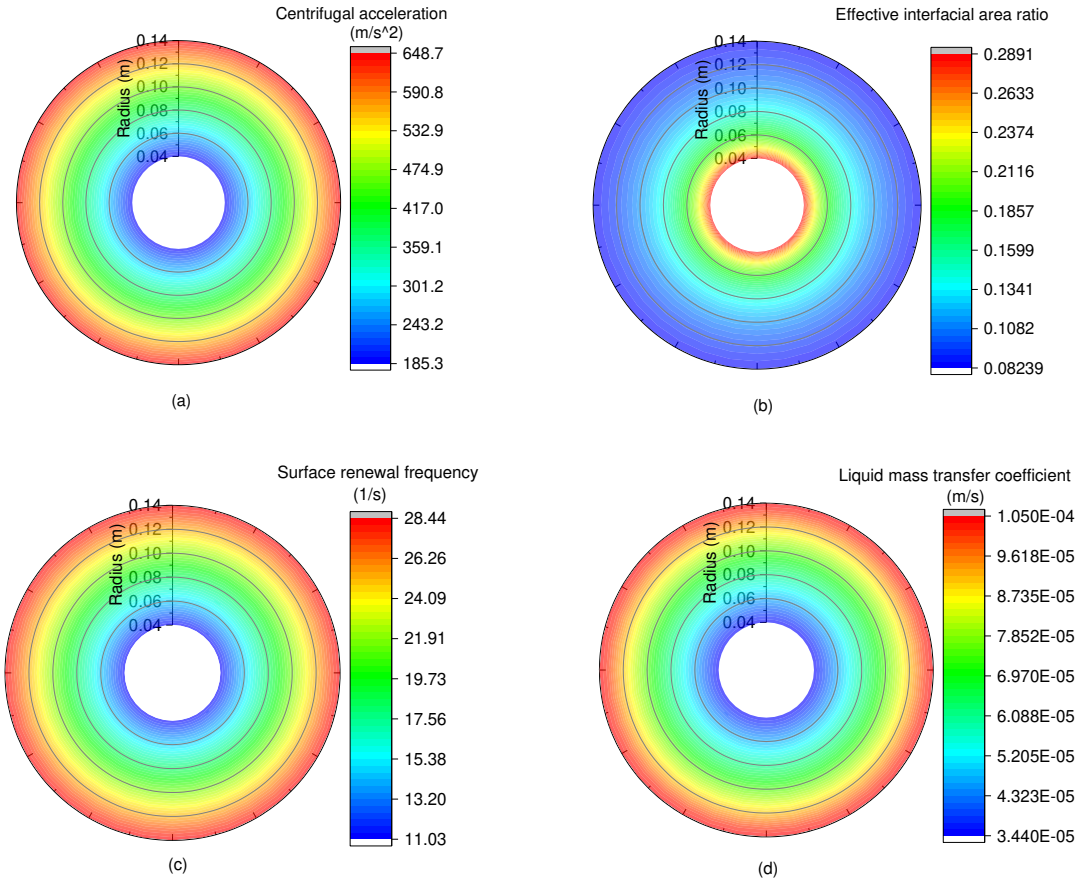

Figure 10. Parameters inside the RPB for base case by process simulation: (a) centrifugal acceleration, (b) effective interfacial area ratio, (c) surface renewal frequency, and (d) liquid mass transfer coefficient

5.2 Case studies through steady state simulation

5.2.1 The effect of rotating speed

Based on the underpinning principle of RPBs, the rotating speed of the motor should have a big impact on absorption performance. In this case study, the rotor speed was varied from 300 rpm to 1450 rpm with other inputs the same as the base case. The aim of this case study is

to understand the relationship between rotating speed and CO_2 absorption performance of the RPB absorber.

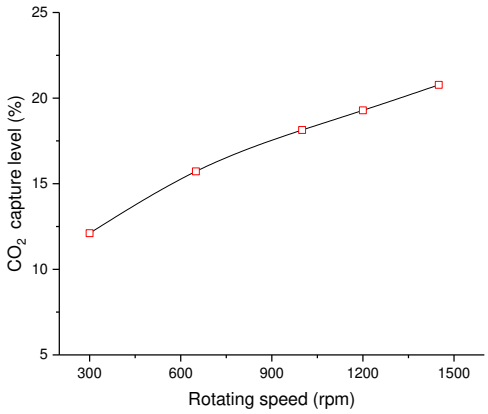

Figure 11. CO_2 capture level in function with rotating speed

Fig.11 presents the effect of varying rotor speed on CO_2 capture level for 50 wt% MEA concentration in the solvent. The results show that CO_2 capture level rises with increase in rotor speed from 300rpm to around 1450rpm. Its trend becomes a little flat at the high rotating speed. It is a result of nonlinear interaction of many variables. Four key variables were plotted in Fig. 12 to tentatively explain the reason. With increasing rotating speed, the centrifugal acceleration increases significantly (seen in Fig.12 (a)). This causes higher surface renewal frequency (seen in Fig.12 (b)) resulting in higher liquid mass transfer coefficient (seen in Fig.12 (c)). However, centrifugal accelerations inside the RPB absorber are as high as 100-350 times Earth's gravity at rotating speeds of 1150-1450 rpm. In this situation, the liquid has lower hold-up and therefore less residence time. As a result, the effective interfacial area ratio decreases at the high rotating speed (seen in Fig.12 (d)). That may be the reason why the increase rate of CO_2 capture level diminishes at the high rotating speed.

Moreover, it can be found that $a_e \propto {a_c}^{-0.533}$ and $k_L \propto {a_c}^{0.74}$ at the inner side of RPB whilst $a_e \propto {a_c}^{-0.526}$ and $k_L \propto {a_c}^{0.783}$ at the outer side of RPB. Thus, the volumetric liquid mass transfer coefficient $k_L a_e \propto {a_c}^{0.207}$ at the inner side of RPB and $k_L a_e \propto {a_c}^{0.257}$ at the outer side of RPB. The proportionality exponents are lower than the study by Vivian, Brian [12]

($k_L a_e \propto {a_c}^{0.41-048}$) and close to the predictions by Chen, Lin [39] ($k_L a_e \propto {a_c}^{0.29}$) and Munjal, Duduković [40] ($k_L a_e \propto {a_c}^{0.315-0.373}$). They also falls in the range of 1/6 -1/3 by the theoretical studies[10, 11].

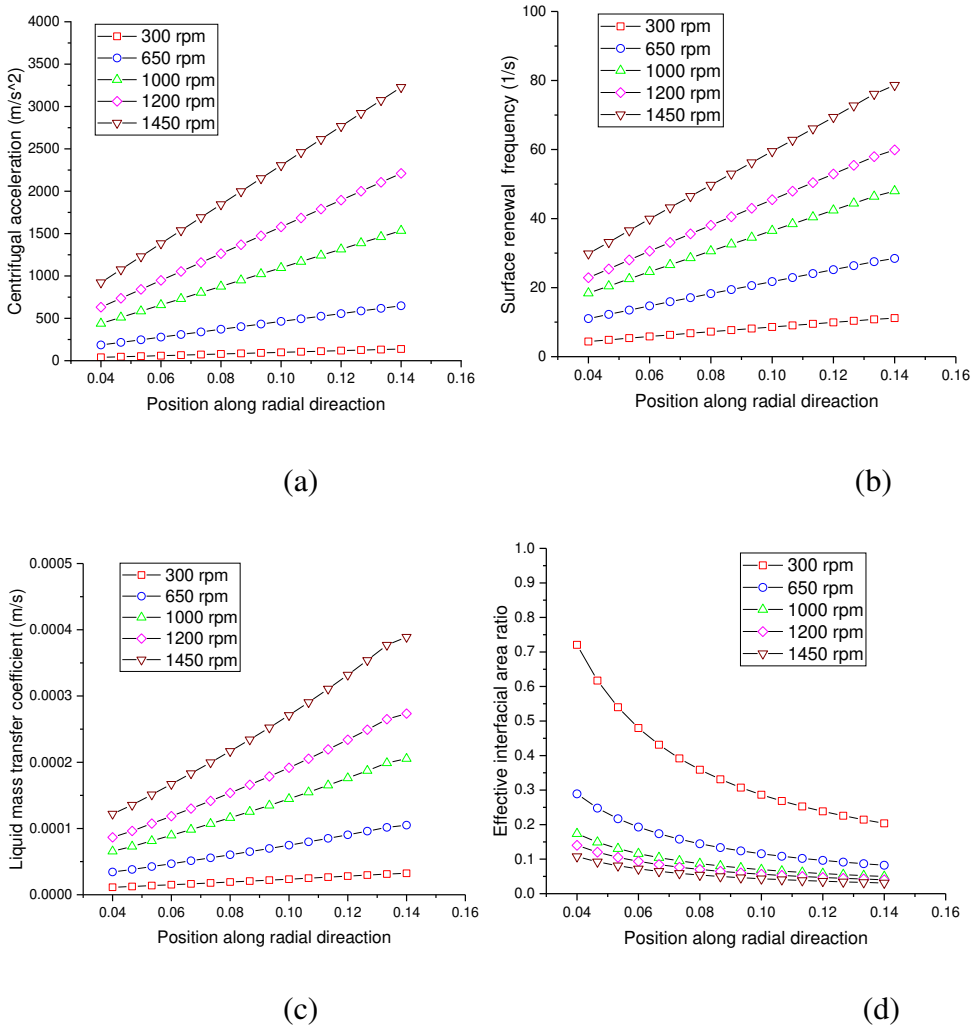

Figure 12. Mass transfer relevant parameters inside the RPB absorber (a) centrifugal acceleration, (b) surface renewal frequency, (c) liquid mass transfer coefficient, and (d) effective interaction area ratio

5.2.2 The Effect of L/G ratio

The L/G ratio has a big impact on the absorption efficiency of the absorber in PCC process. For conventional absorbers, it has been known that the mass transfer performance benefits from increasing L/G ratio. In this case study, the L/G ratio is varied in a range of 2-6 kg/kg with

other inputs consistent with the base case, to investigate the effect of L/G ratio on the performance of the RPB absorber.

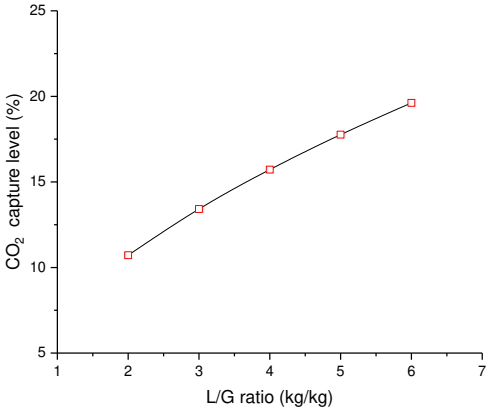

Figure 13. CO_2 capture level in function with L/G ratio in mass

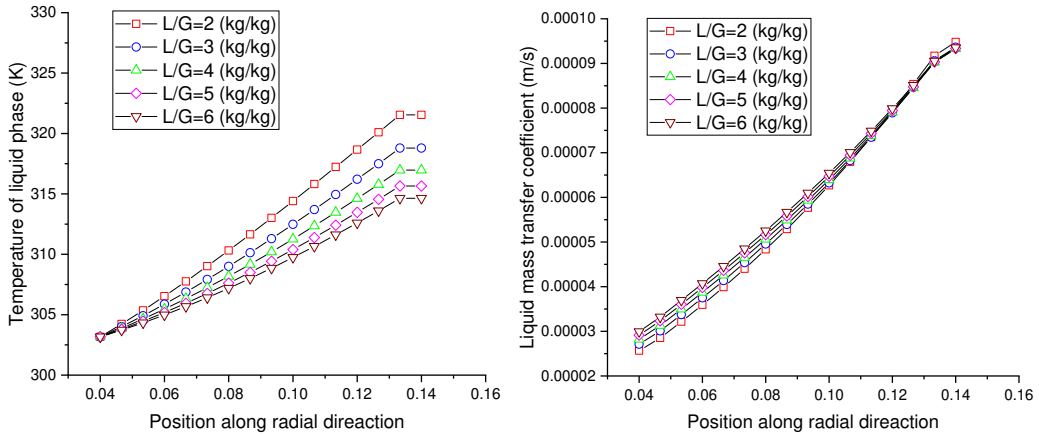

(a)

(b)

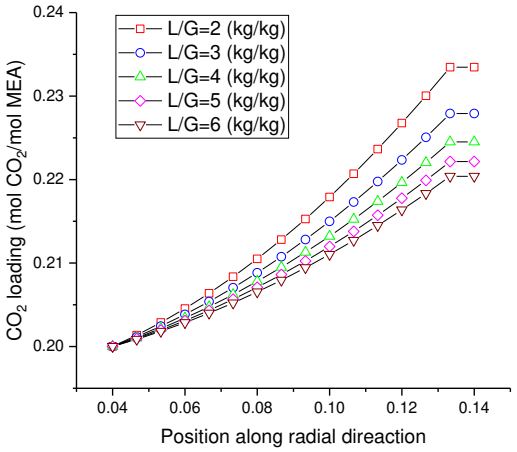

(c)

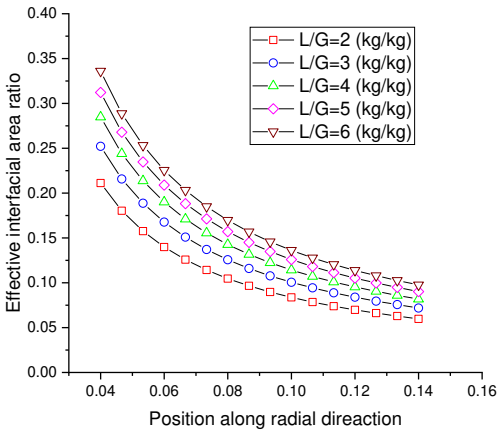

(d)

Figure 14. Mass transfer relevant parameters inside the RPB absorber (a) temperature of liquid phase, (b) liquid mass transfer coefficient, (c) CO_2 loading in liquid phase, and (d) effective interfacial area ratio

Fig.13 shows that CO_2 capture level increases with increase of L/G ratio from 2 to 6 kg/kg. The liquid temperature profile goes down with the increase of L/G ratio ((see Fig.14(a)) due to higher liquid mass flow, which then results in high viscosity. However, higher flow rate of the liquid may enhance the fluid turbulence. Under the coactions of these two factors, the surface renewal frequency decreases slightly with higher L/G ratio. Higher flow rate of liquid phase also shortens the liquid-gas contact time. As a result, liquid mass transfer coefficient increases slightly at high L/G ratios (see Fig.14(b)). Two other major contributors are from changing of CO_2 loading and the effective interfacial area. The increments of CO_2 loading in the liquid shown in Fig.14(c) are not such big because the capture levels are only around 12-20%. If the carbon capture level increases to 90%, CO_2 loading will have more significant impact to the absorption performance. Another effect of higher liquid flow rate is the increasing of effective interfacial area (see Fig.14(d)), which benefits the overall capture efficiency.

5.2.3 The Effect of MEA concentration in solvent

Increased MEA concentration in the solvent leads to higher capture levels but greater tendency for equipment corrosion. A good understanding is needed firstly to explore the optimal range of MEA concentration based on absorption performance of RPBs. In this case study, MEA concentration in the lean solvent was varied from 30 wt% to 80 wt% whilst the flow rate of the lean solvent is kept at 244.8kg/h and other inputs are consistent with the base case.

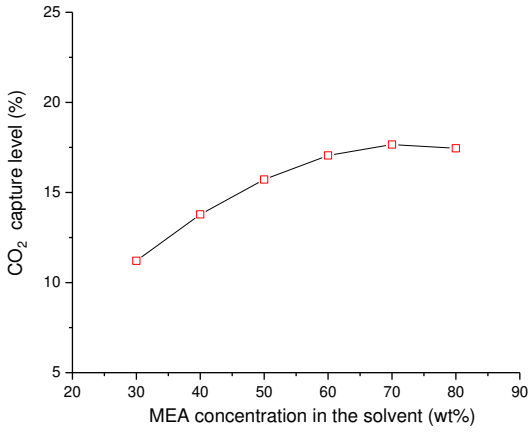

Figure 15. CO_2 capture level in function with MEA concentration in lean solvent

Fig.15 shows that CO_2 capture level increase with the increase of MEA concentration from 30wt% and then reach an optimal point nearby 70wt%. This outcome is consistent with the experimental results. Looking back to Fig.8(a) in Section 4.2, the improvement of CO_2 absorption efficiency from 33wt% MEA solvent to 42wt% MEA solvent is more significant than from 42wt% MEA solvent to 62wt% MEA solvent. In the experimental study by Jassim, Rochelle [13], it is also noticed that the CO_2 efficiency decays for higher MEA concentration (≥70wt%) solvent cases.

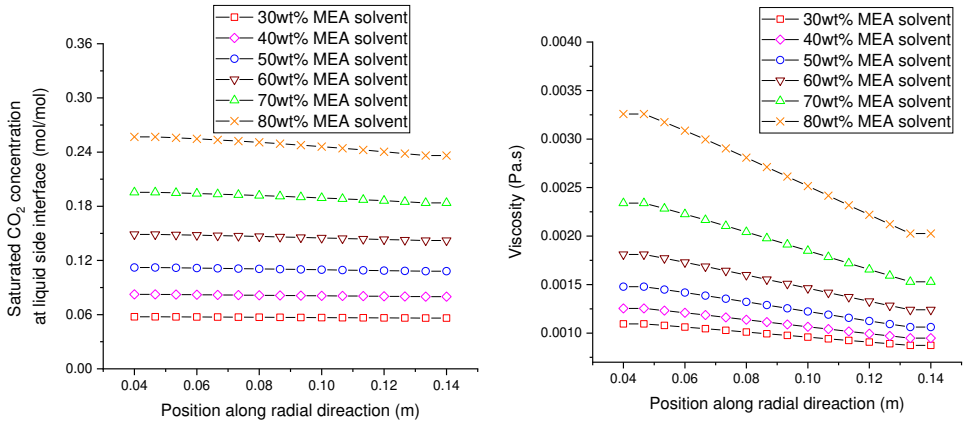

(a) (b)

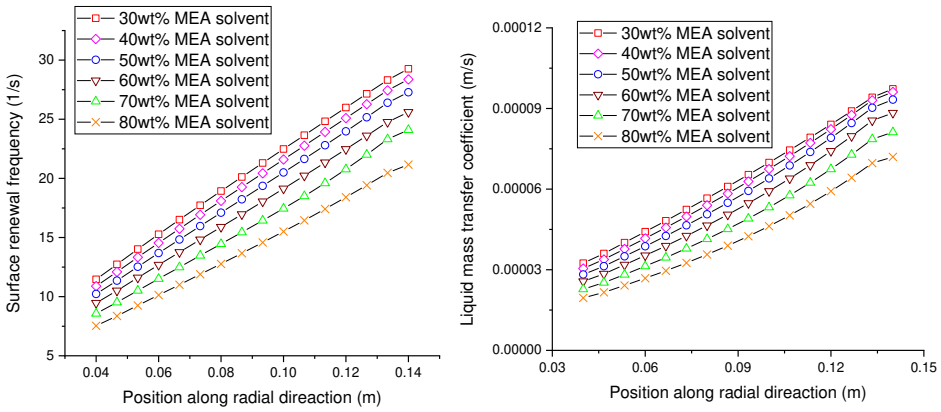

(c) (d)

Figure 16. Mass transfer relevant parameters inside the RPB absorber (a) saturated CO_2 concentration at liquid side interface, (b) liquid viscosity, (c) surface renewal frequency, and (d) liquid mass transfer coefficient

Fig.16 examines the values of key parameters along radial direction. It can be seen that the saturated CO_2 concentration at the liquid-side interface for 80 wt% MEA case is much higher than 30 wt% (see Fig.16 (a)). Higher MEA concentration cases have higher viscosities (see Fig.16 (b)) which leads to lower surface renewal frequencies (see Fig.16 (c)). As a result, the liquid mass transfer coefficients decrease for higher MEA concentration cases (see Fig.16 (d)). The effective interfacial area slightly also decreases at higher MEA concentration cases, due to the increased viscosity of the solvent.

However, other features of the solvent such as foaming, degradation and causticity may change with the increasement of MEA concentration. More studies on this point are meaningful and required for PRB's industry scale applications.

5.3 Case studies through dynamic simulation

The two case studies below explore the dynamic behaviours of the RPB absorber. These replicate typical operations when connected to a power plant.

5.3.1 Decrease of the flow rate of the flue gas

In this case, the flow rate of the flue gas decreases from the load of the base case (100%) to 50% load. There are two possible operation strategies: either keeping same flow rate of the lean solvent or decreasing the flow rate of the lean solvent from 100% to 50% correspondingly. So two operating scenarios were set up for the case study as follows (also illustrated in Fig.17).

•Scenario-A: Change of the flow rate of the flue gas without changing lean MEA flow rate.

•Scenario-B: Change of the flow rate of the flue gas with corresponding change in the flow rate of the lean solvent.

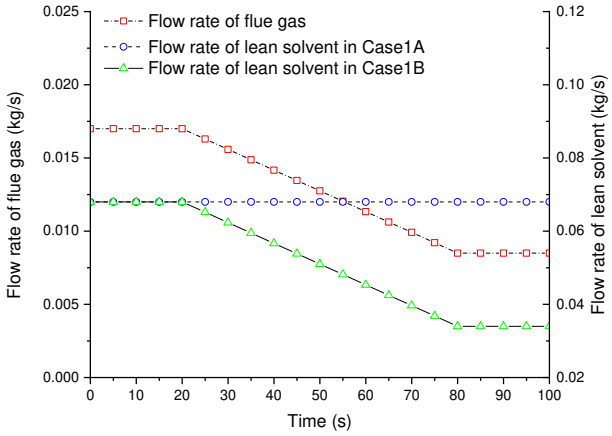

Figure 17. Sketch of changing the flow rates of the flue gas and the lean solvent

Fig. 18 displayed the capture level changing with time for these two scenarios. It is certain that the capture level increases for Scenario-A because keeping same flow rate of lean solvent means L/G ratio increase significantly, which improves the absorption efficiency. In Scenario-B, the liquid and vapour loads per volume of packing actually decrease to 50% although L/G ratio was kept constant. That leads to lower fluid turbulence, resulting in a slight decrease in the liquid mass transfer coefficient. The effective interfacial area ratios also decrease but its decreasing amplitude is much less than 50%. As an overall result, the capture level still slightly increases with same L/G ratio.

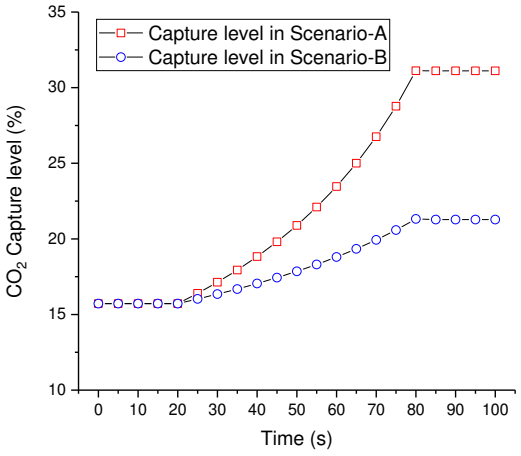

Figure 18. Capture level changes with time

According to the above discussions, one preferable operation strategy for decrease of the flue-gas (for example as power plants switch to low-load operation) is to decrease the flow rate of lean solvent (Scenario-B) for cost saving purpose.

5.3.2 Increasing the flow rate of lean solvent

This case study explored the dynamic performance of increasing the lean solvent flow rate to improve the carbon capture level. Considering short residence time of the liquid inside the RPB absorber that results from small liquid holdup in the pilot-scale rig, the total length of the simulation time is 6 seconds. The flow rate of the lean solvent was ramped from 50% to 100% and then to 150% of the base case, with disturbances introduced at 2 second intervals.

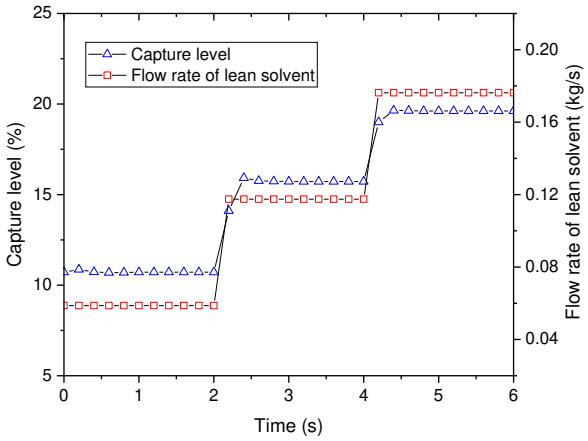

Figure 19. Capture level changes with time when increasing lean solvent flow rate

Fig.19 illustrated the capture level changing with the increase of the lean solvent flow rate. The response time of the system is around 1 seconds before becoming stable, which indicates the RPB absorber has a very fast response time to process disturbance. That is consistent with the experimental observations related with RPB dynamics during the experiments originally designed for study on liquid hold-up inside RPB by Keyvani and Gardner [41] and Burns, Jamil [36]. Compared with static packed column, RPB has smaller equipment size and less liquid hold-up. These two features result in much low total liquid hold-up in RPB, which leads to its fast dynamic. This fast dynamic response is a great advantage for PCC to equip with upstream processes such as gas turbine power plants.

6 Conclusions

This paper presents the development of a novel dynamic model of the RPB absorber for an intensified MEA-based carbon capture process. The RPB absorber model was developed based on surface renewal theory for mass transfer. SAFT-VR EOS was used for the thermodynamic model. The model can predict the distributed mass transfer coefficients and other parameters. The steady state model validation results showed good agreements between model predictions and experimental data for 33, 42% and 62% MEA solvents cases. This provides great confidence in this model as an effective tool for research and design of RPB processes.

Process analysis was performed for the base case initially, to explore the parameters relevant to mass transfer. Case studies were carried out through both steady state and dynamic simulations, using the validated model to investigate the impact of different rotating speeds, L/G ratios and MEA concentrations on the mass transfer performance. The results show that the mass transfer coefficients will increase significantly from inner side to outer side of the RPB absorber whilst the effective interfacial area ratio between liquid and gas reduces with increase of rotating speed of RPBs. The optimal point of MEA concentration is around 70wt%, higher than conventional stationary column. Dynamic simulation of decreasing of the flue gas flowrate, and increasing the lean solvent flow rate, were performed respectively. Simulation

results reveal that the RPB absorber has fast responses, which is a great advantage when carbon capture plant is applied to power plants requiring fast dynamics such as natural gas-fired combined cycle power plants.

Acknowledgement

The authors would like to acknowledge the financial support of EU Systematic Design and Testing of Advanced Rotating Packed Bed Processes and Phase-Change Solvents for Intensified Post-Combustion CO_2 Capture (ROLINCAP) (Project ID: 727503) under the EU H2020 Low Carbon Energy scheme. The authors are also grateful to the UK Engineering and Physical Sciences Research Council (EPSRC) for funding this research (Project Reference Number: EP/M001458/2 and EP/N024672/1).

References

[1] IEA. World Energy Outlook 2017. 2017.
[2] Rochelle GT. Amine Scrubbing for CO_2 Capture. Science. 2009;325:1652-4.
[3] Luo X, Wang M. Optimal operation of MEA-based post-combustion carbon capture for natural gas combined cycle power plants under different market conditions. International Journal of Greenhouse Gas Control. 2016;48, Part 2:312-20.
[4] Mac Dowell N, Shah N. Identification of the cost-optimal degree of CO_2 capture: An optimisation study using dynamic process models. International Journal of Greenhouse Gas Control. 2013;13:44-58.
[5] Ramshaw C, Mallinson RH. Mass transfer process. Google Patents; 1981.
[6] Wang M, Joel AS, Ramshaw C, Eimer D, Musa NM. Process intensification for post-combustion CO_2 capture with chemical absorption: A critical review. Applied Energy. 2015;158:275-91.
[7] Joel AS, Wang M, Ramshaw C, Oko E. Process analysis of intensified absorber for post-combustion CO_2 capture through modelling and simulation. International Journal of Greenhouse Gas Control. 2014;21:91-100.
[8] Podbielniak WJ. Centrifugal counter current contact apparatus. Google Patents; 1935.
[9] Van Krevelen DW, Hoftijzer PJ. Studies of gas absorption: II. Application of the liquid film resistance relationship to the absorption of carbon dioxide by solutions of diethanolamine. Recueil des Travaux Chimiques des Pays-Bas. 1947;66:67-70.
[10] Vivian JE, Peaceman DW. Liquid-side resistance in gas absorption. AIChE Journal. 1956;2:437-43.
[11] Onda K, Sada E, Murase Y. Liquid-side mass transfer coefficients in packed towers. AIChE Journal. 1959;5:235-9.
[12] Vivian JE, Brian PLT, Krukonis VJ. The influence of gravitational force on gas absorption in a packed column. AIChE Journal. 1965;11:1088-91.
[13] Jassim MS, Rochelle G, Eimer D, Ramshaw C. Carbon dioxide absorption and desorption in aqueous monoethanolamine solutions in a rotating packed bed. Industrial and Engineering Chemistry Research. 2007;46:2823-33.

[14] Tung HH, Mah RSH. Modeling liquid mass transfer in higee separation process. Chemical Engineering Communications. 1985;39:147-53.
[15] Munjal S, Dudukovć MP, Ramachandran P. Mass-transfer in rotating packed beds-I. Development of gas-liquid and liquid-solid mass-transfer correlations. Chemical Engineering Science. 1989;44:2245-56.
[16] Oko E, Wang M, Ramshaw C. Study of Mass Transfer Correlations for Intensified Absorbers in Post-combustion CO_2 Capture Based on Chemical Absorption. Energy Procedia. 2017;114:1630-6.
[17] Luo Y, Chu GW, Zou HK, Zhao ZQ, Dudukovic MP, Chen JF. Gas-liquid effective interfacial area in a rotating packed bed. Industrial and Engineering Chemistry Research. 2012;51:16320-5.
[18] Onda K, Takeuchi H, Okumoto Y. Mass transfer coefficients between gas and liquid phases in packed columns. Chem Eng Jap. 1968:1.
[19] Danckwerts PV, Lannus A. Gas‐liquid reactions. Journal of The Electrochemical Society. 1970;117:369C-70C.
[20] Borhani TN, Oko E, Wang M. Process modelling and analysis of intensified CO_2 capture using monoethanolamine (MEA) in rotating packed bed absorber. Journal of Cleaner Production. 2018;204:1124-42.
[21] Burns JR, Ramshaw C. Process intensification: Visual study of liquid maldistribution in rotating packed beds. Chemical Engineering Science. 1996;51:1347-52.
[22] Danckwerts P. Significance of liquid-film coefficients in gas absorption. Industrial & Engineering Chemistry. 1951;43:1460-7.
[23] Neumann K, Gladyszewski K, Groß K, Qammar H, Wenzel D, Górak A, et al. A guide on the industrial application of rotating packed beds. Chemical Engineering Research and Design. 2018;134:443-62.
[24] PSE Ltd. gPROMS ModelBuilder: The world's leading Advanced Process Modelling environment. 2017.
[25] Galindo A, Davies LA, Gil-Villegas A, George J. The thermodynamics of mixtures and the corresponding mixing rules in the SAFT-VR approach for potentials of variable range. Molecular Physics. 1998;93:241-52.
[26] Mac Dowell N, Samsatli NJ, Shah N. Dynamic modelling and analysis of an amine-based post-combustion CO_2 capture absorption column. International Journal of Greenhouse Gas Control. 2013;12:247-58.
[27] Brand CV, Graham E, Rodríguez J, Galindo A, Jackson G, Adjiman CS. On the use of molecular-based thermodynamic models to assess the performance of solvents for CO_2 capture processes: monoethanolamine solutions. Faraday discussions. 2016;192:337-90.
[28] Aronu UE, Gondal S, Hessen ET, Haug-Warberg T, Hartono A, Hoff KA, et al. Solubility of CO_2 in 15, 30, 45 and 60 mass% MEA from 40 to 120°C and model representation using the extended UNIQUAC framework. Chemical Engineering Science. 2011;66:6393-406.
[29] Luo X, Wang M. Improving Prediction Accuracy of a Rate-Based Model of an MEA-Based Carbon Capture Process for Large-Scale Commercial Deployment. Engineering. 2017;3:232-43.
[30] Lawal A, Wang M, Stephenson P, Koumpouras G, Yeung H. Dynamic modelling and analysis of post-combustion CO_2 chemical absorption process for coal-fired power plants. Fuel. 2010;89:2791-801.
[31] Oyenekan BA, Rochelle GT. Alternative stripper configurations for CO_2 capture by aqueous amines. AIChE Journal. 2007;53:3144-54.
[32] Cussler EL. Diffusion: mass transfer in fluid systems: Cambridge university press; 2009.

[33] Shen Z, Xu W, Ding J. Interphase mass transfer-A revised model for Surface Renewal Theory. Journal of Chemcial Industry and Engineering (China). 1980;4:319-32.
[34] Versteeg GF, van Swaaij WPM. Solubility and Diffusivity of Acid Gases (CO_2, N_2O) in Aqueous Alkanolamine Solutions. Journal of Chemical and Engineering Data. 1988;33:29-34.
[35] Deng B, Dai G. Numerical simulation of surface renewal frequency on vertically rotating disc. CIESC Journal. 2015;65:116-22.
[36] Burns JR, Jamil JN, Ramshaw C. Process intensification: operating characteristics of rotating packed beds — determination of liquid hold-up for a high-voidage structured packing. Chemical Engineering Science. 2000;55:2401-15.
[37] Kister HZ, Haas JR, Hart DR, Gill DR. Distillation design: McGraw-Hill New York; 1992.
[38] Chang YC. Potentiometric Titration of Free Amine and Amine Carbonate in Carbonated Monoethanolamine Solutions. Analytical Chemistry. 1958;30:1095-7.
[39] Chen Y-S, Lin C-C, Liu H-S. Mass Transfer in a Rotating Packed Bed with Viscous Newtonian and Non-Newtonian Fluids. Industrial & Engineering Chemistry Research. 2005;44:1043-51.
[40] Munjal S, Dudukovi ć MP, Ramachandran P. Mass-transfer in rotating packed beds-II. Experimental results and comparison with theory and gravity flow. Chemical Engineering Science. 1989;44:2257-68.
[41] Keyvani M, Gardner N. Operating characteristics of rotating beds. Technical progress report for the third quarter 1988. Case Western Reserve Univ., Cleveland, OH (United States). Dept. of Chemical Engineering; 1988.